

See discussions, stats, and author profiles for this publication at: <https://www.researchgate.net/publication/317733859>

Phosphoproteomic profiling reveals ALK and MET as novel actionable targets across synovial sarcoma subtypes

Article *in* Cancer Research · June 2017

DOI: 10.1158/0008-5472.CAN-16-2550

CITATIONS

0

READS

22

23 authors, including:



Emmy D G Fleuren

Institute of Cancer Research

23 PUBLICATIONS 202 CITATIONS

[SEE PROFILE](#)



Vijesh Vaghjiani

Monash University (Australia)

34 PUBLICATIONS 468 CITATIONS

[SEE PROFILE](#)



Jason E. Cain

Hudson Institute

47 PUBLICATIONS 584 CITATIONS

[SEE PROFILE](#)



Yvonne M H Versleijen-Jonkers

Radboud University Medical Centre (Radboudu...)

38 PUBLICATIONS 319 CITATIONS

[SEE PROFILE](#)

Some of the authors of this publication are also working on these related projects:



Changes in Culture Expanded Human Amniotic Epithelial Cells: Implications for Potential Therapeutic Applications [View project](#)

Phosphoproteomic profiling reveals ALK and MET as novel actionable targets across synovial sarcoma subtypes

[Emmy D.G. Fleuren](#)^{1,2†}, [Myrella Vlenterie](#)^{3†}, [Winette T.A. van der Graaf](#)^{1,4}, [Melissa H.S. Hillebrandt-Roeffen](#)³, [James Blackburn](#)^{5,6}, [Xiuquan Ma](#)⁷, [Howard Chan](#)⁷, [Mandy C. Magias](#)⁷, [Anke van Erp](#)³, [Laurens van Houdt](#)³, [Sabri A.S. Cebeci](#)³, [Amy van de Ven](#)³, [Uta E. Flucke](#)⁸, [Erin E. Heyer](#)⁵, [David M. Thomas](#)⁹, [Christopher J. Lord](#)², [Kieren D. Marini](#)¹⁰, [Vijesh Vaghjiani](#)¹⁰, [Tim R. Mercer](#)^{5,6}, [Jason E. Cain](#)¹⁰, [Jianmin Wu](#)^{9,11}, [Yvonne M.H. Versleijen-Jonkers](#)³ and [Roger J. Daly](#)⁷

[†] *These authors contributed equally*

Authors' affiliations:

¹ Division of Clinical Studies, The Institute of Cancer Research, London, United Kingdom

² The CRUK Gene Function Laboratory and the Breast Cancer Now Toby Robins Breast Cancer Research Centre, The Institute of Cancer Research, London, United Kingdom

³ Department of Medical Oncology, Radboud University Medical Centre, Nijmegen, The Netherlands

⁴ Royal Marsden NHS Foundation Trust, London, United Kingdom

⁵ Genomics and Epigenetics Division, Garvan Institute of Medical Research, Sydney, New South Wales, Australia

⁶ St. Vincent's Clinical School, Faculty of Medicine, UNSW, Sydney, New South Wales, Australia

⁷ Cancer Research Program, Biomedicine Discovery Institute and Department of Biochemistry and Molecular Biology, Monash University, Clayton, VIC 3800, Australia

⁸ Department of Pathology, Radboud University Medical Centre, Nijmegen, the Netherlands

⁹ Cancer Division, The Kinghorn Cancer Centre, Garvan Institute of Medical Research, Sydney, NSW 2010, Australia

¹⁰ Centre for Cancer Research, Hudson Institute of Medical Research and Department of Molecular and Translational Science, Monash University, Clayton, Victoria, Australia

¹¹ Key laboratory of Carcinogenesis and Translational Research (Ministry of Education/Beijing), Center for Cancer Bioinformatics, Peking University Cancer Hospital & Institute, Hai-Dian District, Beijing 100142, China

Running title: Phosphoproteomic profiling of sarcomas

Keywords: Signal transduction, Ewing sarcoma, angiosarcoma, rhabdomyosarcoma, GIST

Funding: EDG Fleuren is supported with a travel grant from the Dutch Cancer Society (KWF) and a Rubicon Fellowship from the Netherlands Organisation for Scientific Research (NWO; 019.153LW.035). RJ Daly is supported by a Fellowship (1058540) from the National Health and Medical Research Council of Australia. YMH Versleijen-Jonkers and WTA van der Graaf are supported by the Synovial Sarcoma Research Foundation and the Radboud AYA foundation. J Wu is supported by SRF for ROCS, State Education Ministry (SEM), and Young Talents Program, Beijing Municipal Administration of Hospitals.

Corresponding authors and contact information:

Emmy D.G. Fleuren

Gene Function Laboratory and Clinical Studies

The Institute of Cancer Research

237 Fulham Road, London SW3 6JB, United Kingdom

Phone: 0044 020 7153 5035

E-mail: Emmy.Fleuren@icr.ac.uk

Roger J. Daly

Department of Biochemistry and Molecular Biology

Monash University

Level 1, Building 77, Clayton Campus

23 Innovation Walk

Clayton VIC 3800

Australia

Phone: 0061 3 990 29301

E-mail: roger.daly@monash.edu

Potential conflicts of interest: The authors declare no potential conflicts of interest

Word count: 4505

Total number of tables and figures: 7 original (1 table, 6 figures)

References: 50

Abstract

Despite intensive multi-modal treatment of sarcomas, a heterogeneous group of malignant tumors arising from connective tissue, survival remains poor. Candidate-based targeted treatments have demonstrated limited clinical success, urging an unbiased and comprehensive analysis of oncogenic signaling networks to reveal therapeutic targets and personalized treatment strategies. Here we applied mass spectrometry-based phosphoproteomic profiling to the largest and most heterogeneous set of sarcoma cell lines characterized to date and identified novel tyrosine phosphorylation patterns, enhanced tyrosine kinases in specific subtypes, and potential driver kinases. ALK was identified as a novel driver in the Aska-SS synovial sarcoma (SS) cell line via expression of an ALK variant with a large extracellular domain deletion (ALK^{Δ2-17}). Functional ALK dependency was confirmed *in vitro* and *in vivo* with selective inhibitors. Importantly, ALK immunopositivity was detected in 6/43 (14%) of SS patient specimens, one of which exhibited an ALK rearrangement. High PDGFR α phosphorylation also characterized SS cell lines, which was accompanied by enhanced MET activation in Yamato-SS cells. Although Yamato-SS cells were sensitive to crizotinib (ALK/MET-inhibitor) but not pazopanib (VEGFR/PDGFR-inhibitor) monotherapy *in vitro*, synergistic effects were observed upon drug combination. *In vivo*, both drugs were individually effective, with pazopanib efficacy likely attributable to reduced angiogenesis. MET or PDGFR α expression was detected in 58% and 84% of SS patients, respectively, with co-expression in 56%. Consequently, our integrated approach has led to the identification of ALK and MET as promising therapeutic targets in SS.

Introduction

Sarcomas are a heterogeneous group of malignant tumors arising in the bone or other connective tissue. Despite multi-modal treatment options comprising intensive polychemotherapy, radiotherapy and surgery, the survival of advanced sarcoma patients, with the exception of those exhibiting gastro-intestinal stromal tumors (GIST), has not improved substantially during the last decade (1,2), and side effects may affect quality of life. This emphasizes the need for novel, targeted systemic therapies. In recent years, the specific targeting of oncogenic signaling proteins with either small-molecule tyrosine kinase inhibitors (TKIs) or antibodies has been the subject of numerous preclinical and clinical studies in sarcoma. Of these, only the multi-kinase VEGFR/PDGFR/KIT-inhibitor pazopanib showed an increase in progression-free survival (PFS) in a phase III study, leading to its registration in advanced non-adipocytic soft-tissue sarcoma (STS) after failure of standard treatment (3), and a phase I-II study with the PDGFR α antibody olaratumab led to an impressive but not yet understood overall survival improvement (4). Possible explanations for the observed limited clinical efficacy are: inclusion of a wide variety of sarcoma subtypes per study without incorporation of predictive biomarkers (2,5); and use of single inhibitors rather than combinations, since numerous studies demonstrate that tumors often rely on multiple signaling pathways to maintain growth and progression (1,2,6-8). Therefore, there is a critical need to define, at a global level, the activated signaling networks that drive sarcoma progression, determine how they relate to currently-defined sarcoma subtypes and whether they can provide a novel taxonomy for the disease, and identify targeted therapies and companion biomarkers for implementation of personalized treatment approaches.

So far, genetic screening underpins diagnosis of different sarcoma subtypes, yet targetable driver mutations are rarely found in non-GIST sarcomas. While disease-specific translocations such as EWS-ETS in Ewing sarcomas (ES) and SS18-SSX in synovial sarcomas (SS) have been demonstrated (9), the exact cellular functions of these fusions and their potential relationship to other oncogenic events is not fully understood, and targeting the translocation or associated activated pathways has not yet

been successful. Therefore, mutation screening to select non-GIST sarcoma patients for targeted therapy has not led to clinical benefit so far (1,10,11). Regarding protein biomarkers, most studies to date have focused on total protein expression levels, while specific screening for phosphorylation status or other read-outs of activation state may provide more accurate information regarding the pathway dependency of tumor cells and likely therapeutic benefit (2,12,13,14). To this end, we characterized tyrosine kinase signaling networks in a large panel of sarcoma cell lines ($n=20$). We specifically chose to include sarcoma cell lines of both the bone sarcoma and STS subtypes, and sarcomas occurring in adults or at pediatric/adolescent or young adult (AYA) age (Table 1). Except for the GIST cell line, none of the included cell lines have been phosphoprofiled before, and this is the first study to subject SS and angiosarcoma (AS) cell lines to phosphoproteomic analysis (6,15). This has enabled us to (1) characterize activated signaling networks in sarcoma (2) compare activated signaling networks between and within sarcoma subtypes and (3) identify driver kinases. The results highlight potential strategies for future personalized sarcoma treatment.

Materials and Methods

Cell culture: ES and RMS cell lines were kindly provided by Peter Houghton, SS cell lines by Kazuyuki Itoh (Yamato-SS and Aska-SS), Akira Kawai (SYO-1) and Cinzia Lanzi (CME-1); AS cell lines by Mikio Masuzawa (MO-LAS-B and ISO-HAS-B) and the GIST cell line by Jonathan Fletcher (GIST882). All cell lines were obtained between 2010-2015, authenticated in our laboratory upon arrival and routinely tested for mycoplasma (all negative). All translocation-associated cell lines (ES, SS and aRMS) were authenticated in our laboratory by confirming the presence of the characteristic EWS-FLI1 (ES), SS18-SSX1/SSX2 (SS), or PAX3-FKHR (aRMS) gene fusions as listed in Table 1 by RT-PCR. Fusion-negative eRMS cell lines were additionally tested for PAX3-FKHR gene fusions, which all proved to be fusion-negative, as expected. For the GIST882 cell line, mutation analysis confirmed its known KIT mutation (K642E; c.1924A>G=p.Lys642Glu). AS and eRMS cell lines were tested by immunohistochemistry (IHC) for the presence of subtype-specific protein markers, which included expression of CD31, CD34 and ERG for AS cell lines, and expression of desmin and myogenin for eRMS cell lines. Authentication methods and results of all cell lines were reviewed by an expert sarcoma pathologist (UE Flucke, Radboud UMC). Cells were cultured according to their recommended conditions to approximately 70% confluency for no longer than 25 passages in total for any experiment.

Phosphoproteomic profiling: Prior to profiling studies, cells were harvested and homogenized in 8M urea lysis buffer containing phosphatase inhibitors. Lysates were sonicated and centrifuged at 14,000 g at 4°C for 20. For each cell line, 20 mg of protein was subjected to phosphoproteomic analysis. First, phosphopeptides were immunoprecipitated (details: Supplementary Methods). For nanoscale liquid chromatography coupled to tandem mass spectrometry (nano LC-MS/MS) analysis, pY-peptides were resuspended in MS-loading buffer (0.1% formic acid and 2% ACN). Peptides were separated over a 30 min. gradient and MS was performed using a Thermo Fisher Scientific (San Jose, CA, USA) Orbitrap Plus. Up to the 10 most abundant ions (>5,000 counts) with charge states > +2

were sequentially isolated and further subjected to MS/MS fragmentation. MS data were analyzed using MaxQuant software (version 1.5.2.8.). Extracted peak lists were searched against the human UniProtKB/Swiss-Prot database (version 2010_10), concatenated with a proportionally sized decoy database for false discovery rate (FDR) as well as the reversed sequences of all entries. Protein, peptide, and site FDRs were controlled at a maximum of 1%. Raw pY-peptide spectral intensities were extracted from the 'Evidence' output files generated by Maxquant. These intensities were normalised against pY-peptide intensities for the heavy-labelled spiked-in peptide standards combined with GSK3B. The label-free intensity values of EFTU, MK14 and GSK3B heavy peptides in each cell line were averaged and a subsequent normalization factor generated. MS intensity values of each pY-site quantified in the dataset were divided by the appropriate normalization factor. Raw MaxQuant output files were subjected to the following stringent filtering criteria prior to inclusion in bioinformatics analysis; 1) contaminants and reversed matches were removed, ensuring all identifications had a FDR of <1%, 2) all non-pY-sites (serine and threonine) were removed, 3) pY-sites were filtered for a minimum localization probability confidence of 0.75. All data was log₂ transformed prior to bioinformatics analysis. Data analyses were performed using Microsoft Office Excel and the bioinformatics platform Perseus (Max Planck Institute of Biochemistry, Munich) version 1.2.0.19. For hierarchical clustering, only pY-sites with at least 10 valid values were included, according to standard Perseus filtering and clustering criteria.

Pathway and network analysis: For pathway enrichment analysis, the KEGG Orthology Based Annotation System (KOBAS) was used (16). The hypergeometric test was applied to test statistical enrichment of identified KEGG and Reactome pathways, and the p-values were corrected for multiple comparisons using the Benjamini and Hochberg method (17). Physical interactions among proteins of interest were retrieved from the Protein Interaction Network Analysis (PINA) platform (18,19), and kinase-substrate relationships were downloaded from the PhosphoSitePlus database (20). The networks were generated and visualized using PINA4MS, a Cytoscape plugin for PINA.

Proliferation assays: The effects of small-molecule inhibitors (TAE684, crizotinib, ceritinib and pazopanib) on cell viability was assessed by MTT-proliferation assays as previously described (21,22)(details: Supplemental Table 1).

Patient cohort: Tumor samples from 43 patients diagnosed with SS (all SS18-SSX translocation positive) between 1988 and 2015, were retrieved from the files of the department of Pathology of the Radboud University Medical Centre (Radboud UMC). Patient follow-up data was retrieved from the clinical records. The study was performed in accordance with the Code of Conduct of the Federation of Medical Scientific Societies in the Netherlands. Patient characteristics are listed in Supplemental Table 2.

FISH: Fluorescent *in situ* hybridization (FISH) was performed on 2 μ m-thick formalin-fixed paraffin embedded (FFPE) tissue microarray (TMA) sections from the patient cohort described above, and an Aska-SS cytopsin using an ALK (2p23) split-signal FISH DNA probe (Dako) as previously described (21).

Mutation analysis: RT-PCR and sequence analysis of the RTK domain of ALK and MET was performed on SS cell lines as described previously (21). SS cells were additionally screened with the Cancer Hotspot Panel with a focus on potential PDGFR α and EGFR mutations (23).

Sequencing Library preparation and Capture: Sequencing libraries were prepared from 1 μ g of Aska-SS RNA using the KAPA Stranded RNA-Seq Library Preparation Kit (Roche). Capture was performed using biotinylated probes complementary to the *ALK* coding regions as previously described (24) with addition of the double Capture process according to manufacturer's instructions. Captured libraries were sequenced for standard depth 126bp paired-end sequencing using the Illumina HiSeq 2500 System v4 (Illumina).

Sequence Analysis: Sequencing reads were deduplicated with Tally v15-065 and adaptor sequences removed with Cutadapt v1.8.1. Post-filtering, reads were mapped to human reference genome hg38

with STAR v2.4.2a and converted to UCSC genome browser tracks using the BEDTools v2.25.0 'genomcov' command. *ALK* exonic coverage was calculated from uniquely-mapping reads using the BEDTools coverage tool (details: Supplementary Methods).

ALK RT-PCR: 1 µg of total RNA was reverse-transcribed to DNA using the High-Capacity cDNA Reverse Transcription Kit (Applied Biosystems). PCR was performed using the primer sequences listed in the Supplementary Methods. Products were gel-purified using the Gel and PCR Clean-Up System (Promega) and were sequenced using the PCR primers.

Western Blot: Western Blot analysis was performed as previously described (25)(antibody details: Supplemental Table 3).

PathScan analysis: PathScan signaling analysis was performed on Aska-SS cells treated with TAE684 (25 nM), ceritinib (100 nM) or crizotinib (750 nM) and on Yamato-SS cells treated with pazopanib (10 µM) and/or crizotinib (750 nM), all for 24h, using the human PathScan RTK signaling antibody array kit (Cell Signaling Technology) according to the manufacturer's protocol.

Deglycosylation: Cells were lysed in 2% SDS and the lysates adjusted to 0.5% SDS, 40 mM DTT and centrifuged at 12,000 g for 10 min at room temperature. The supernatant was then heated at 96°C for 10 min and 10 µg of protein treated with *O*-Glycosidase, Endoglycosidase H, N-glycosidase F (all from NEB), following manufacturer's protocols. Tunicamycin was obtained from Sigma. Cells were incubated with tunicamycin (2.5-20 µg/ml) for 24 h prior to preparation of cell lysates and Western blotting.

Combination indices: To assess drug synergy between crizotinib and pazopanib, the combination index (CI) method was used (22). Cells were treated with three designated doses of crizotinib (20, 50 and 100 nM) and pazopanib (100, 1,000 and 10,000 nM), and effects on cell viability were assessed by MTT assays. We next identified concentrations of each monotherapy necessary to obtain a similar

reduction in cell viability as observed with combined treatments. Subsequently, CI for the combination treatments was calculated using the formula $CI = [C_{a,x}/IC_{x,a}] + [C_{b,x}/IC_{x,b}]$. $C_{a,x}$ and $C_{b,x}$ are the concentrations of drugs A and B used in combination to achieve x% drug effect, $IC_{x,a}$ and $IC_{x,b}$ are concentrations for single agents to achieve the same effects. A CI < 1 indicates synergy of the combination therapy. A CI equal to or higher than 1 indicates additivity or antagonism, respectively.

Soft-agar colony forming assays: Soft-agar colony forming assays were performed as previously described (25).

Mouse xenografts: Animal study protocols were performed in accordance with the guidelines of the Institutional Animal Welfare Committee of the Radboud University Nijmegen and Monash University. 5×10^6 - 1×10^7 cells of Yamato-SS or Aska-SS cells were subcutaneously inoculated into 6–7-week-old female BALB/c mice ($n=6-9$ per group). Drug administration was initiated when tumors were palpable. Crizotinib, ceritinib and pazopanib were suspended in 0.5% hydroxypropylmethylcellulose (HPMC) + 0.5% Tween-80 to the necessary concentrations. For dose-response experiments, mice bearing Yamato-SS tumors were randomized into four groups receiving either crizotinib (0mg/kg, 12.5mg/kg, 25mg/kg or 50mg/kg) once daily or pazopanib (0mg/kg, 10mg/kg, 30mg/kg or 100mg/kg) twice daily, both orally. Mice bearing Aska-SS tumors were treated with either vehicle or 50 mg/kg of crizotinib or ceritinib once daily. Tumor growth was measured twice weekly with calipers. After 28 days of treatment, all mice were sacrificed and the resected tumors were fixed in formalin.

Immunohistochemistry: Immunohistochemistry of MET, PDGFR α and ALK on SS patient TMAs and CD34 and Ki67 staining on SS tumor xenografts was performed as previously described (21,26)(Antibody details: Supplemental Table 3). Patient characteristics are listed in Supplemental Table 2.

Affymetrix analysis: ALK, MET and PDGFR α mRNA transcript levels were extracted from a publically-available Affymetrix dataset (accession number GDS2736) of 105 clinical STS specimens (including 16 SS) to compare mRNA transcript levels between sarcoma subgroups.

Results

Phosphotyrosine profiling of human sarcoma cell lines

Our cell line panel comprised 20 different sarcoma cell lines, including adult (AS and GIST) and pediatric/AYA (ES, RMS and SS) sarcomas (Table 1). Note that even though SS can occur at all ages, all cell lines were derived from young adult patients. Tyrosine phosphorylation patterns were characterized by an immunoaffinity-coupled LC-MS/MS workflow, and after application of stringent filter criteria (see Methods), we identified 1090 tyrosine phosphorylated peptides corresponding to 654 proteins. Of these 1090 peptides, 334 met criteria for inclusion in subsequent hierarchical clustering analyses (Methods and Supplemental Table 4). Upon unsupervised hierarchical clustering of the different sarcoma cell lines based on their tyrosine phosphopeptide profile, the cell lines clustered into two major groups, being the adult sarcomas (GIST and AS) (designated Subgroup A) and the pediatric/AYA sarcomas (SS, RMS and ES) (Figure 1A). Since the large pediatric/AYA cluster split into the ES4 cell line and two smaller clusters, we have designated the latter two pediatric/AYA clusters Subgroups B and C, respectively (Figure 1A). Note that in this subclassification, cell lines of particular sarcoma subtypes do not always cluster together. The majority of the ES cell lines are split between Subgroups B and C. In addition, examples of RMS lines were also found in these two Subgroups, and this subclassification was not explained by their aRMS (translocation-positive; Table 1) or eRMS (translocation-negative) status. However, the SS cell lines clustered together in Subgroup B.

In order to identify signaling networks that exhibited differential activity across novel Subgroups A-C, an ANOVA-based approach was applied to identify Subgroup-enriched phosphosites, followed by bioinformatic determination of protein-protein interaction networks or pathways associated with these sites (27). Subgroup A was characterized by hyperphosphorylation of 48 phosphosites, with significant enrichment for the pathways associated with Fc gamma receptor (FCGR)-dependent phagocytosis, EPH-Ephrin signaling, adherens junctions and cytoskeletal organization (Supplemental

Table 5). Protein-protein interaction analysis for the proteins corresponding to these phosphosites revealed a network with the key hubs PTK2 (focal adhesion kinase; FAK) and ACTB (β -actin) (Figure 1B). Other kinases present within this network were FGR, MAPK3, TYRO3, and YES1. The only phosphosite significantly enriched in Subgroup B versus the other two subgroups was PKP4 Y478, while Subgroup C was characterized by significant hypophosphorylation of 48 sites compared to Subgroups A and B. The protein-protein interaction network corresponding to these hypophosphorylated sites exhibited major hubs associated with PI3K signaling (PIK3R1, PIK3R2), and this approach also emphasized the decreased phosphorylation of certain kinases (PDGFR α , EPHA2 and JAK2) in Subgroup C versus the other Subgroups (Supplemental Figure 1).

Next, tyrosine kinases (TKs) were extracted from the original dataset, since these represent an important class of oncogenes and druggable targets (14). This resulted in the identification of 132 phosphotyrosine peptides belonging to 41 TKs, including 26 receptor tyrosine kinases (RTKs) and 15 non-receptor TKs (Supplemental Table 4). Unsupervised hierarchical clustering based on the tyrosine kinase-derived phosphopeptides resulted in a more complex pattern than that generated using all phosphopeptides, but served to highlight ALK and KIT as highly-phosphorylated 'outliers' in the Aska-SS and GIST882 cell lines, respectively, that may act as drivers (Figure 1C). To facilitate comparison between different (R)TKs, the total tyrosine phosphorylation count was calculated per protein (see Methods) (Figure 2A). For RTKs, ALK, EPHA2 and KIT contributed the greatest proportion of phosphopeptide counts across the panel (although this reflects major contributions from individual cell lines for ALK and KIT, Figure 2B), whilst for non-receptor TKs, FAK, LYN, SRC and YES made the largest contributions (Figure 2A). Considering the phosphorylation patterns across the panel, the non-receptor TKs SRC/LYN/YES, FAK1 and the RTK EPHA2 were phosphorylated at high levels in the majority of cell lines (Figure 2B). Some tyrosine kinases exhibited enhanced phosphorylation in subsets of cell lines without a clear preference towards a specific sarcoma subtype (e.g. EPHB3 in ES7, RH18, Rh36 and Aska-SS). Certain kinases appeared to be more sarcoma subtype-specific, as exemplified by increased phosphorylation of DDR2 in ES cells, FGFR4 in RMS, EGFR, EPHA7 and

PDGFR α in SS and lastly TIE1, VEGFR2, FGR, and BMX in AS. As expected, the GIST882 cell line exhibited an exceptionally high level of KIT phosphorylation (Figure 2B), reflecting its KIT-driven phenotype and imatinib sensitivity (28). Interestingly, an extreme phosphotyrosine content was observed for ALK in the Aska-SS cell line, suggesting a novel and yet undescribed role for ALK as an oncogenic driver in SS.

ALK represents a novel driver in SS

In addition to the marked ALK tyrosine phosphorylation in Aska-SS, our MS analyses detected low ALK tyrosine phosphorylation on specific sites in ES2, EW8, Rh3 and Rh5. However, only Aska-SS cells demonstrated detectable phosphorylation on the ALK activation loop residues Y 1278, 1282 and 1283 (29) (Supplemental Table 4). Western blotting detected expression of full-length ALK (220 kDa) in several sarcoma cell lines, including ES7, EW8, Rh41 and Rh3 (Supplemental Figure 2), whereas Aska-SS expressed two predominant anti-ALK immunoreactive bands of ~110 and 80 kDa (Figure 2C). Importantly, these aberrant ALK proteins in Aska-SS were detected using ALK-antibodies directed to pY1096, Y1507 and Y1282/1283, with highest phosphorylation levels in the 110 kDa variant (Figure 2C). The latter observation particularly applied to activation loop phosphorylation. These data indicated that Aska-SS cells express truncated, activated ALK proteins, and suggested the 110 kDa variant represents the major driver. To determine the origin of these aberrant proteins, FISH analysis was undertaken, which identified heterozygous ALK breakage in Aska-SS cells (Figure 3A). RNAseq using an ALK Capture panel did not detect an ALK fusion partner, but instead revealed discontinuous coverage of ALK exons, with low expression from exon 1, absent expression from exons 2-17, and the majority of expression from exon 18 onwards (Figure 3B). RT-PCR confirmed the presence of mRNA transcripts where exon 1 (containing the usual initiation codon) is spliced to exon 18 (Figure 3C-D). These would encode an aberrant ALK protein lacking the extracellular region encoded by exons 2-17, designated ALK Δ 2-17 (Figure 3E and Supplemental Figure 3) with a predicted molecular weight of approximately 100 kDa. Since the larger ALK immunoreactive band in Aska-SS was approximately 110

kDa, we determined whether the size difference between this and the predicted product was due to glycosylation. Treatment of Aska-SS lysate with endoglycosidase H, which targets high mannose-containing immature N-linked carbohydrates, resulted in partial conversion of the 110 kDa band to a 100 kDa form (Supplemental Figure 4A), while incubation with O-Glycosidase resulted in a small but reproducible increase in mobility. However, treatment with N-glycosidase F, which removes almost all types of N-linked (Asn-linked) glycosylation, resulted in complete conversion to a 100 kDa form consistent with the predicted size for ALK Δ 2-17. This also resulted in a shift of the 80 kDa ALK band to approximately 70 kD. The 70 kDa form is consistent with use of initiation sites within exon 18, or alternatively this may represent a cleaved version of the larger variant. Treatment of cells with tunicamycin, an inhibitor of N-linked glycosylation, confirmed the impact of this modification on mobility of ALK Δ 2-17 (Supplemental Figure 4B). ALK mutation analysis in the other SS cell lines demonstrated a previously reported ALK exon 23 deletion in Yamato-SS cells. This is known to also occur in RMS and ES, and has no effect on crizotinib sensitivity (20, 30, 31).

To determine the functional role of ALK in SS, the effect of a panel of ALK inhibitors including the clinically-used compounds crizotinib (ALK/MET) and ceritinib (ALK), and the tool compound TAE684 (ALK), on cell proliferation was determined (Figure 4A and Supplemental Table 6). Aska-SS cells were extremely sensitive to all three inhibitors, with IC_{50} values ranging between 26-46 nM. The other three SS cell lines exhibited markedly lower sensitivity to TAE684 and ceritinib, reflecting their lack of ALK activation. Yamato-SS cells were also sensitive to crizotinib, likely explained by high levels of MET activation, consistent with their sensitivity to the MET/VEGFR2 inhibitor foretinib (Figure 4A and Supplemental Figure 5). Crizotinib IC_{50} values were substantially higher for SYO-1 and CME-1 cells which exhibit undetectable or very low levels of ALK/MET tyrosine phosphorylation (Figure 2B). Western Blot and PathScan analysis determined that the ALK inhibitors decreased ALK phosphorylation in Aska-SS cells and in general, significantly reduced activation of Erk, Akt, S6RP, STAT3 and STAT1 (Figure 4B-C). Prolonged treatment resulted in decreased expression of Cyclin A, Rb

hypophosphorylation and PARP cleavage, consistent with increased cell-cycle arrest in G₁ and enhanced apoptosis (Supplemental Figure 6). Importantly, treatment of mice bearing subcutaneous Aska-SS xenografts with either crizotinib or ceritinib demonstrated a remarkable dependency on ALK for tumor growth and maintenance, with drug treatment resulting in robust and durable tumor regressions (Figure 4D-E). Histopathology analyses demonstrated that these regressions were associated with a significant decrease in the number and size of tumor blood vessels, as well as less proliferative cells (Supplemental Figure 7). Overall these data demonstrate that ALK Δ 2-17 activates multiple proliferative and survival pathways resulting in ALK addiction both *in vitro* and *in vivo*.

To confirm the clinical relevance of these findings, we first interrogated a publically-available Affymetrix dataset of 105 clinical STS specimens (including 16 SS) and compared ALK mRNA transcript levels between sarcoma subgroups. This determined that ALK mRNA was significantly more highly expressed in SS as compared to other STS, suggesting a unique and specific role for ALK in SS versus other STS subtypes (Supplemental Figure 8). In addition, we assessed protein expression of ALK in 43 primary SS patient specimens. ALK immunopositivity was observed in 6/43 (14%) of the patients (Figure 4F-G, Supplemental Figure 9). No significant correlation was found between ALK expression levels and patient outcome. The ALK-expressing samples were also evaluated by FISH. Interestingly, one of the six ALK-positive patients showed ALK rearrangement in 23% of the cells (100 cells counted; Figure 4H). This prompted us to evaluate an additional four metastatic lesions from the same patient. All lesions were positive for ALK expression. FISH analysis reported translocations in 10-15.3% of cells in three of the lesions (50-150 cells counted per lesion, depending on lesion size). The fourth lesion showed ALK gain of up to 6 copies. These data validate our cell line-based *in vitro* and *in vivo* studies and highlight ALK as an important therapeutic target in a subset of SS.

Kinase activation profiles and rational design of combination therapies

Although the phosphoproteomic analysis identified driver kinases in Aska-SS and GIST882 cell lines, the other sarcoma cell lines often exhibited more than one TK with high levels of activation (Figure 1A and 2B). One way to overcome the problem of network 'robustness' conferred by multiple activated kinases is implementation of combination treatments or use of appropriate multi-kinase inhibitors (25). Again, we focused on the SS cell lines to further test this hypothesis. In addition to aberrant ALK activation in Aska-SS, these lines were characterized by high MET (in Yamato), and PDGFR α and EGFR phosphorylation in all of the lines (Figure 2B). No mutations were found in MET, PDGFR α or EGFR in any of the SS cell lines. PDGFR- or EGFR-targeted monotherapies proved ineffective *in vitro*, with at best modest growth suppression with the VEGF/PDGFR inhibitor pazopanib in SYO-1 cells (Figure 5A, Supplemental Figure 5 and Supplemental Table 6). Therefore, we determined whether simultaneous targeting of one of these kinases might enhance the observed sensitivity of Yamato-SS cells to the ALK/MET inhibitor crizotinib (Figure 4A). Given the robust expression of PDGFR α in Yamato-SS cells (Figure 5B), and the fact that pazopanib is clinically approved for SS treatment, this was undertaken with pazopanib. Interestingly, synergistic effects (CI<0.8) were observed upon combined treatment with pazopanib and crizotinib (Figure 5C), indicating that targeting PDGFR α is effective but only in the context of MET inhibition. Western Blot and PathScan signaling analysis revealed that Erk activation was sensitive to crizotinib but not pazopanib, and determined that combination treatment significantly reduced Akt S473 and STAT1 Y701 phosphorylation compared to each monotherapy and control, providing potential mechanisms for the observed drug synergy (Figure 5D-E). Combination treatment also resulted in enhanced apoptosis, as indicated by the appearance of cleaved PARP at 48 h post-treatment (Supplemental Figure 10). Combined treatment with crizotinib and pazopanib was also significantly more effective than either monotherapy in soft-agar colony forming assays (Figure 5F).

However, in mice bearing subcutaneous Yamato-SS xenografts, we observed a dose-dependent tumor growth retardation with each compound individually, which was more pronounced with crizotinib (Figure 5G-H). Crizotinib-treated tumours were characterized by significant reductions in

blood vessel size (mean CD34+ vessel surface for vehicle, 176.8 mm²/vessel vs. crizotinib 50mg/kg, 129.3 mm²/vessel, p=0.0261) and tumor cell mitotic count (vehicle, 3.1±0.9 vs. crizotinib 50mg/kg, 0.8±0.3, p=0.0057). Therefore, Yamato-SS cells exhibit a dependency on MET for tumor growth *in vivo*. In pazopanib-treated tumors, there were significantly fewer CD34+ blood vessels compared to controls (vehicle, 189.7/mm² vs. pazopanib 100mg/kg, 122.2/mm²; p=0.0073; Figure 5I). This effect on angiogenesis, likely mediated by VEGFR inhibition, probably underpins the contrasting sensitivity of Yamato-SS cells to pazopanib treatment *in vitro* and *in vivo*. Overall, these data demonstrate that MET represents a potential therapeutic target in a subset of SS, indicate that pazopanib may also be of benefit for specific SS patients, and highlight the potential clinical utility of crizotinib/pazopanib combination treatment.

MET and PDGFR α expression in SS patients

To interrogate MET and PDGFR α expression in SS patients, we utilized publically-available Affymetrix gene expression data and also assayed our own cohort of clinical SS specimens by IHC. There was no significant difference for MET mRNA expression in SS compared to the other sarcoma histologies, but there was a trend for higher PDGFR α mRNA expression in SS (Supplemental Figure 8). Immunopositivity for MET or PDGFR α was detected in 58% (25/43) and 84% (36/43) of SS patients, respectively (Figure 6A-B). In 56% (24/43) of SS patients, the two proteins were co-expressed, but the highest scores for PDGFR α and MET were mutually exclusive. Interestingly, two of the patients presenting with the histological biphasic SS subtype showed a remarkable differential MET/PDGFR α co-expression pattern, with MET and PDGFR α expressed mutually exclusively in distinct areas of the tumor resembling the epithelial and spindle cell components characteristic of this subtype (Figure 6C). These data confirm that MET and PDGFR α represent potential therapeutic targets in SS, either alone or in combination.

Discussion

In this study, we utilized mass-spectrometry-based phosphoproteomics to profile the largest and most heterogeneous set of sarcoma cell lines screened to date in order to identify perturbed signaling networks characteristic of existing or novel subtypes, and driver kinases that may represent candidate therapeutic targets. Importantly, this has identified several potential therapeutic strategies for specific subsets of SS patients, highlighting opportunities for personalized treatment of this sarcoma subtype.

Our study identified ALK as a novel driver in the Aska-SS cell line, with exceptionally high ALK tyrosine phosphorylation levels similar to those of the driver kinase KIT in the imatinib-sensitive GIST882 cell line (28). We determined that the ALK sensitivity in Aska-SS was underpinned by expression of a novel truncated ALK variant lacking a significant proportion of the extracellular domain (ALK Δ 2-17). Other activated ALK variants with extracellular domain deletions have been described in neuroblastoma and melanoma, where the deletions encompass regions encoded by exons 2-3, and all of the extracellular domain, respectively (32,33). Consequently our data add to growing evidence that extracellular domain deletions unleash the oncogenic potential of ALK, and represent a significant mechanism for ALK deregulation in human cancers, in addition to mutation, fusion and gene amplification/overexpression (29).

Although all SS tumors harbor SS18-SSX fusion genes, there is a wide variety in clinical behavior and response to chemotherapy or targeted treatment within these tumors, emphasizing the role of additional factors in orchestrating SS progression (34). Our detection of ALK Δ 2-17 in the Aska-SS cell line, and an ALK rearrangement in an ALK-immunopositive SS patient specimen, highlight ALK alterations as one such factor. Because the ALK aberration was detected in 1/4 SS cell lines and 1/43 SS patients, yet all of our SS samples and cell lines harbored the characteristic SS18-SSX translocation, ALK is likely not associated with the characteristic SS18-SSX fusion gene. In addition, since the Aska-SS cell line harbors SS18-SSX1, while the patient specimen contained SS18-SSX2, ALK aberrations are

not associated with expression of a specific SS18-SSX fusion. Since ALK activation in STS has been linked to the presence of metastatic lesions (35), Aska-SS is derived from a pulmonary metastatic lesion, and the ALK breakage-positive SS patient demonstrated breakage-positive metastases, ALK aberration in SS may be required for metastatic progression. However, it is clear from our comprehensive functional analyses in Aska-SS that ALK signaling is required for cell proliferation and survival *in vitro*, and tumor growth and maintenance *in vivo*. Consequently, once ALK activation occurs, the cancer cells can become dependent on this driver, despite the presence of a SS18-SSX fusion.

We acknowledge that ALK-targeted treatment will likely not be applicable to SS tumors in general, but the dependency of a subset of these tumors on ALK-signaling offers great potential for personalized treatment within this sarcoma subtype. In this regard, ALK protein expression was detected in 14% of primary SS tumors and 1/6 of the ALK immunopositive-tumors exhibited ALK rearrangement, with the percentage of breakage-positive cells meeting diagnostic criteria for designation as ALK aberration-positive. The presence of a small subpopulation of SS patients exhibiting these characteristics is similar to non-small cell lung cancer (NSCLC), where ALK rearrangements are found in 2-7% of cases (36). In the latter setting, oncogenic ALK fusions are an established companion biomarker for crizotinib sensitivity. In addition, IC₅₀ values for crizotinib in Aska-SS cells were similar to those of ALK-rearranged lymphoma cells, where ALK is an established clinical target (37). Consequently our work highlights ALK as an oncogenic driver and highly-promising therapeutic target in a subset of SS.

ALK has also been assessed as a therapeutic target in other sarcoma subtypes. A phase I dose-escalation study of crizotinib for pediatric cancer patients, including a variety of sarcoma subtypes, reported enriched anti-tumor activity in patients with inflammatory myofibroblastic tumors (IMT). Here, the impressive response rate in this subtype was attributed to the presence of activating ALK aberrations. No ALK aberrations or objective responses to crizotinib were reported in other sarcoma

subtypes, although no SS patients were included (38). In addition to IMT, RMS have been subject to clinical evaluation of crizotinib efficacy based on reported ALK protein expression and gene amplification (NCT01548926, NCT02034981 and NCT01742286) (31). However, no objective responses have been reported in RMS patients (39,40). These data may reflect a failure to detect genomic ALK rearrangements in this subtype. Furthermore, while we could detect ALK expression in certain RMS cell lines, this was not accompanied by relevant levels of ALK phosphorylation, indicating that ALK protein overexpression in RMS may not be accompanied by receptor activation.

Three other RTKs demonstrated enhanced activation in SS cell lines, MET in Yamato-SS, and PDGFR α and EGFR in all SS lines. Importantly, Yamato-SS cells were sensitive to crizotinib *in vitro* and *in vivo*, and over half of primary SS tumors demonstrated MET expression, highlighting MET as a potential therapeutic target in this sarcoma subtype. In the case of PDGFR α and EGFR, treatment of SS cells with pazopanib, gefitinib or erlotinib was without effect *in vitro*, indicating that these RTKs do not act as sole drivers. However, pazopanib exhibited efficacy against Yamato-SS xenografts, likely reflecting an additional effect on VEGFRs leading to reduced angiogenesis. The latter data are consistent with pazopanib monotherapy demonstrating clinical benefit in a subset of SS patients, with 49% of the patients having stable disease at 3 months (41). Also, in the extended phase III trial, there was a trend for SS patients to have superior responses on pazopanib, though this was not significant, possibly due to the relatively small size of this subgroup (3). Clearly, our data and recent clinical studies highlight the therapeutic potential for pazopanib in SS, but further work is required to identify biomarkers of therapeutic response that allow administration in a personalized fashion.

Two additional aspects of our study are worthy of comment. First, we determined that a high proportion of clinical SS specimens co-express both MET and PDGFR α , with a subset of biphasic tumors exhibiting differential localization of these receptors to the epithelial and spindle cell components of the tumor, respectively. Although at this point we could not assess phosphorylated protein expression status with IHC on our clinical dataset, these data validate the presence of high levels of these receptors in subsets of SS patients. Second, combined treatment of Yamato-SS cells

with pazopanib and crizotinib demonstrated synergistic effects *in vitro* and in anchorage-independent growth assays, consistent with the high expression and activation of both MET and PDGFR α . Although the expression of MET has been described previously in SS, explicitly in the epithelial part (42-43), its combination with PDGFR α expression in spindle cell parts in biphasic tumors is novel, as is the combination of MET and PDGFR α targeting. Consequently, our work highlights a potential combination therapy that could be used for SS tumors that co-express MET and PDGFR α , either in the same tumor region, or in a biphasic fashion. In this context, it is worth noting that two phase I studies in other advanced cancers are running: NCT01468922, combining the MET-inhibitor ARQ197 with pazopanib; and NCT01548144, combining pazopanib with crizotinib. A preliminary case report of the latter study reported a therapeutic response and good tolerability of the combined treatment at the lowest doses (200mg pazopanib with 250mg crizotinib) (44), emphasizing its clinical potential.

Beyond SS, the global and unbiased nature of our phosphoproteomic profiling approach enabled us to identify potential therapeutic targets for other sarcoma subtypes, including DDR2 in ES and FGFR4 in RMS. In addition, molecular subclassification based on tyrosine phosphorylation patterns led to a novel taxonomy, with the pediatric/AYA sarcomas clustering away from adult sarcomas and subdivided into two subgroups. In this subclassification, cell line models of the ES and RMS sarcoma subtypes do not cluster together in their designated ES and RMS histological classifications, respectively, highlighting how knowledge of histological subtype is insufficient for assigning targeted treatments, and further molecular interrogation is required to design more personalized approaches. To this end, detailed signaling network analyses identified hyper- and hypophosphorylation signatures characteristic of each of the novel subgroups, revealing that the hyperphosphorylation pattern in Subgroup A (adult sarcomas) is built around a network with PTK2 (FAK) as a key component, potentially identifying FAK as a specific, and actionable vulnerability in these tumors. Importantly, a number of small molecule FAK tyrosine kinase inhibitors are currently undergoing pre-clinical and clinical testing. In particular, PF-00562271, VS-4718 and VS-6063 demonstrated promising

clinical activity in patients with selected solid cancers, emphasizing their potential utility for sarcoma treatment (45, 46).

Of note, the potential of phosphoproteomic screening of sarcomas in the clinic is underlined by recent studies: in a clinical (not further specified) sarcoma sample, phosphoproteomics was capable of detecting an ALK-rearrangement (47), as we did in the Aska-SS cell line, and this technique has also enabled patient stratification in RMS (48). For clinical samples, the use of reverse-phase protein arrays (RPPAs) or Nanostring technology may offer a practical approach for interrogating phosphorylation status when limited amounts of tissue are available (48). The coupling of phosphoproteomic approaches with other established techniques in clinical trial design and accompanying translational studies may therefore be of great value in design of personalized sarcoma treatments (49). The potential power of a phosphoproteomics approach over genomic analyses in SS is exemplified by the study of Ishibashi et al., in which pALK expression was detected in SS cases without underlying genomic aberrations (35).

In conclusion, our study has provided detailed insights into the signaling network characteristics of particular sarcoma subtypes and identified potential therapeutic targets that have been validated using both *in vitro* and *in vivo* models and patient specimens. This work has identified protein and phosphoprotein markers that, following further validation, could be incorporated into pathological characterization of sarcomas leading to improved patient stratification for targeted treatment approaches.

Acknowledgements

We thank Peter Houghton of the Pediatric Preclinical Testing Program (PPTP; Columbus, Ohio, USA) for generously providing the ES and RMS cell lines, and Mikio Masuzawa (Kitasato University School of Allied Sciences, Sagamihara, Japan; MO-LAS-B and ISO-HAS-B) and Jonathan Fletcher (Harvard Medical School, Boston, MA, USA; GIST882) for donating the AS and GIST cell lines, respectively. Akira Kawai (National Cancer Center Hospital, Tokyo, Japan; SYO-1), Kazuyuki Itoh and Norifumi Naka (Osaka Medical Center for Cancer and Cardiovascular Diseases, Osaka, Japan; Yamato-SS and Aska-SS), and Cinzia Lanzi (Fondazione IRCCS Istituto Nazionale dei Tumori, Milan, Italy; CME-1) for kindly providing the SS cell lines. Luxi Zhang, Emily Humphrey, Oded Kleifeld, Jim Su and Mark del Borgo provided excellent technical advice and support. We thank the Synovial Sarcoma Research Foundation, Dutch Cancer Society, Radboud AYA foundation, the National Health and Medical Research Council of Australia and the Netherlands Organisation for Scientific Research (NWO; Rubicon) for their financial support.

References

1. [Linch M, Miah AB, Thway K, Judson IR, Benson C. Systemic treatment of soft-tissue sarcoma—gold standard and novel therapies. *Nat Rev Clin Oncol* 2014;11:187-202.](#)
2. [Fleuren ED, Versleijen-Jonkers YM, Boerman OC, van der Graaf WT. Targeting receptor tyrosine kinases in osteosarcoma and Ewing sarcoma: current hurdles and future perspectives. *Biochim Biophys Acta* 2014;1845:266-76.](#)
3. [van der Graaf WT, Blay JY, Chawla SP, Kim DW, Bui-Nguyen B, Casali PG, et al. Pazopanib for metastatic soft-tissue sarcoma \(PALETTE\): a randomised, double-blind, placebo-controlled phase 3 trial. *Lancet* 2012;379:1879-86.](#)
4. [Tap WD, Jones RL, Van Tine BA, Chmielowski B, Elias AD, Adkins D et al. Olaratumab and doxorubicin versus doxorubicin alone for treatment of soft-tissue sarcoma: an open-label phase 1b and randomised phase 2 trial. *Lancet* 2016;388\(10043\):488-97.](#)
5. [Lee AT, Pollack SM, Huang P, Jones RL. Phase III Soft Tissue Sarcoma Trials: Success or Failure? *Curr Treat Options Oncol*. 2017;18:19.](#)
6. [Bai Y, Li J, Fang B, Edwards A, Zhang G, Bui M, et al. Phosphoproteomics identifies driver tyrosine kinases in sarcoma cell lines and tumors. *Cancer Res* 2012;72:2501-11.](#)
7. [Wang X, Goldstein D, Crowe PJ, Yang M, Garrett K, Zeps N, et al. Overcoming resistance of targeted EGFR monotherapy by inhibition of STAT3 escape pathway in soft tissue sarcoma. *Oncotarget* 2016;7\(16\):21496-509.](#)
8. [Potratz J, Tillmanns A, Berning P, Korsching E, Schaefer C, Lechtape B, et al. Receptor tyrosine kinase gene expression profiles of Ewing sarcomas reveal ROR1 as a potential therapeutic target in metastatic disease. *Mol Oncol* 2015; 10\(5\):677-92.](#)
9. [Taylor BS, Barretina J, Maki RG, Antonescu CR, Singer S, Ladanyi M. Advances in sarcoma genomics and new therapeutic targets; *Nat Rev Cancer* 2011;11:541-57.](#)
10. [Italiano A, Di Mauro I, Rapp J, Pierron G, Auger N, Alberti L, et al. Clinical effect of molecular methods in sarcoma diagnosis \(GENSARC\): a prospective, multicentre, observational study. *Lancet Oncol* 2016; 17\(4\):532-8.](#)
11. [Vlenterie M, Hillebrandt-Roeffen MH, Flucke UE, Groenen PJ, Tops BB, Kamping EJ, et al. Next generation sequencing in synovial sarcoma reveals novel gene mutations. *Oncotarget* 2015;6:34680-90.](#)
12. [Fleuren ED, Versleijen-Jonkers YM, van de Luijngaarden AC, Molkenboer-Kueneen JD, Heskamp S, Roeffen MH, et al. Predicting IGF-1R therapy response in bone sarcomas: immuno-SPECT imaging with radiolabeled R1507. *Clin Cancer Res* 2011;17:7693-703.](#)
13. [Dolai S, Sia KC, Robbins AK, Zhong L, Heatley SL, Vincent TL, et al. Quantitative phosphotyrosine profiling of patient-derived xenografts identifies therapeutic targets in pediatric leukemia. *Cancer Res* 2016 \[Epub ahead of print\].](#)
14. [Fleuren ED, Zhang L, Wu J, Daly RJ. The kinome 'at large' in cancer. *Nat Rev Cancer* 2016;16:83-98.](#)
15. [Nagata K, Kawakami T, Kurata Y, Kimura Y, Suzuki Y, Nagata T, et al. Augmentation of multiple protein kinase activities associated with secondary imatinib resistance in gastrointestinal stromal tumors as revealed by quantitative phosphoproteome analysis. *J Proteomics* 2015;115:132-42.](#)
16. [Wu J, Mao X, Cai T, Luo J, Wei L. KOBAS server: a web-based platform for automated annotation and pathway identification. *Nucleic Acids Res* 2006;34 \(Web Server issue\):W720-4.](#)
17. [Benjamini and Hochberg. Controlling the False Discovery Rate - a Practical and Powerful Approach to Multiple Testing. *J.R. Statist Soc* 1995; B 57: 289–300](#)
18. [Wu J, Vallenius T, Ovaska K, Westermarck J, Mäkelä TP, Hautaniemi S. Integrated network analysis platform for protein-protein interactions. *Nat Methods* 2009;6\(1\):75-7.](#)

19. [Cowley MJ, Pinese M, Kassahn KS, Waddell N, Pearson JV, Grimmond SM, et al. PINA v2.0: mining interactome modules. *Nucleic Acids Res* 2012;40\(Database issue\):D862-5.](#)
20. [Hornbeck PV, Zhang B, Murray B, Kornhauser JM, Latham V, Skrzypek E. PhosphoSitePlus, 2014: mutations, PTMs and recalibrations. *Nucleic Acids Res* 2015;43\(Database issue\):D512-20.](#)
21. [Fleuren ED, Roeffen MH, Leenders WP, Flucke UE, Vlenterie M, Schreuder HW, et al. Expression and clinical relevance of MET and ALK in Ewing sarcomas. *Int J Cancer* 2013;133:427-36.](#)
22. [Fleuren ED, Hillebrandt-Roeffen MH, Flucke UE, Te Loo DM, Boerman OC, van der Graaf WT, et al. The role of AXL and the in vitro activity of the receptor tyrosine kinase inhibitor BGB324 in Ewing sarcoma. *Oncotarget* 2014;5:12753-68.](#)
23. [Eijkelenboom A, Kamping EJ, Kastner-van Raaij AW, Hendriks-Cornelissen SJ, Neveling K, Kuiper RP, et al. Reliable Next-Generation Sequencing of Formalin-Fixed, Paraffin-Embedded Tissue Using Single Molecule Tags. *J Mol Diagn* 2016;18:851-863.](#)
24. [Mercer TR, Clark MB, Crawford J, Brunck ME, Gerhardt DJ, Taft RJ, et al. Targeted sequencing for gene discovery and quantification using RNA CaptureSeq. *Nat Protoc* 2014;9:989-1009.](#)
25. [Hochgräfe F, Zhang L, O'Toole SA, Browne BC, Pinese M, Porta Cubas A, et al. Tyrosine phosphorylation profiling reveals the signaling network characteristics of Basal breast cancer cells. *Cancer Res* 2010;70\(22\):9391-401.](#)
26. [Fleuren ED, Versleijen-Jonkers YM, Roeffen MH, Franssen GM, Flucke UE, Houghton PJ, et al. Temsirolimus combined with cisplatin or bevacizumab is active in osteosarcoma models. *Int J Cancer* 2014;135:2770-82.](#)
27. [Humphrey ES, Su SP, Nagrial AM, Hochgräfe F, Pajic M, Lehrbach GM, et al. Resolution of Novel Pancreatic Ductal Adenocarcinoma Subtypes by Global Phosphotyrosine Profiling. *Mol Cell Proteomics* 2016;15\(8\):2671-85.](#)
28. [Tuveson DA, Willis NA, Jacks T, Griffin JD, Singer S, Fletcher CD, et al. STI571 inactivation of the gastrointestinal stromal tumor c-KIT oncoprotein: biological and clinical implications. *Oncogene* 2001;20:5054-8.](#)
29. [Hallberg B, Palmer RH. Mechanistic insight into ALK receptor tyrosine kinase in human cancer biology. *Nat Rev Cancer* 2013;13:685-700.](#)
30. [de Figueiredo-Pontes LL, Wong DW, Tin VP, Chung LP, Yasuda H, Yamaguchi N, et al. Identification and characterization of ALK kinase splicing isoforms in non-small-cell lung cancer. *J Thorac Oncol* 2014;9:248-53.](#)
31. [van Gaal JC, Flucke UE, Roeffen MH, de Bont ES, Sleijfer S, Mavinkurve-Groothuis AM, et al. Anaplastic lymphoma kinase aberrations in rhabdomyosarcoma: clinical and prognostic implications. *J Clin Oncol* 2012;30:308-15.](#)
32. [Okubo J, Takita J, Chen Y, Oki K, Nishimura R, Kato M et al. Aberrant activation of ALK kinase by a novel truncated form ALK protein in neuroblastoma. *Oncogene* 2012;31:4667-4676.](#)
33. [Wiesner T, Lee W, Obenauf AC, Ran L, Murali R, Zhang QF, et al. Alternative transcription initiation leads to expression of a novel ALK isoform in cancer. *Nature* 2015;526:453-7.](#)
34. [Vlenterie M, Jones RL, van der Graaf WT. Synovial sarcoma diagnosis and management in the era of targeted therapies. *Curr Opin Oncol* 2015;27:316-22.](#)
35. [Ishibashi Y, Miyoshi H, Hiraoka K, Arakawa F, Haraguchi T, Nakashima S, et al. Anaplastic lymphoma kinase protein expression, genetic abnormalities, and phosphorylation in soft tissue tumors: Phosphorylation is associated with recurrent metastasis. *Oncol Rep* 2015;33:1667-74.](#)
36. [Kwak EL, Bang YJ, Camidge DR, Shaw AT, Solomon B, Maki RG, et al. Anaplastic lymphoma kinase inhibition in non-small-cell lung cancer. *N Engl J Med* 2010;363:1693-703.](#)

37. [Christensen JG, Zou HY, Arango ME, Li Q, Lee JH, McDonnell SR, et al. Cytoreductive antitumor activity of PF-2341066, a novel inhibitor of anaplastic lymphoma kinase and c-Met, in experimental models of anaplastic large-cell lymphoma. *Mol Cancer Ther* 2007;6:3314-22.](#)
38. [Mossé YP, Lim MS, Voss SD, Wilner K, Ruffner K, Laliberte J, et al. Safety and activity of crizotinib for paediatric patients with refractory solid tumours or anaplastic large-cell lymphoma: a Children's Oncology Group phase 1 consortium study. *Lancet Oncol* 2013;14:472-80.](#)
39. [Vassal G, Faivre L, Geoerger B, Plantaz D, Auvrignon A, Coze C, et al. Crizotinib in children and adolescents with advanced ROS1, MET, or ALK-rearranged cancer: Results of the AcSé phase II trial. *J Clin Oncol* 2016;34 \(suppl; abstr 11509\).](#)
40. [Geoerger B, Schulte J, Zwaan CM, Casanova M, Fischer M, Moreno L, et al. Phase I study of ceritinib in pediatric patients \(Pts\) with malignancies harboring a genetic alteration in ALK \(ALK+\): Safety, pharmacokinetic \(PK\), and efficacy results. *J Clin Oncol* 2015;33 \(suppl; abstr 10005\).](#)
41. [Sleijfer S, Ray-Coquard I, Papai Z, Le Cesne A, Scurr M, Schoffski P, et al. Pazopanib, a multikinase angiogenesis inhibitor, in patients with relapsed or refractory advanced soft tissue sarcoma: a phase II study from the European organisation for research and treatment of cancer-soft tissue and bone sarcoma group \(EORTC study 62043\). *J Clin Oncol* 2009;27:3126-32.](#)
42. [Kuhnen C, Tolnay E, Steinau HU, Voss B, Muller KM. Expression of c-Met receptor and hepatocyte growth factor/scatter factor in synovial sarcoma and epithelioid sarcoma. *Virchows Archiv* 1998;432:337-42.](#)
43. [Oda Y, Sakamoto A, Saito T, Kinukawa N, Iwamoto Y, Tsuneyoshi M. Expression of hepatocyte growth factor \(HGF\)/scatter factor and its receptor c-MET correlates with poor prognosis in synovial sarcoma. *Hum Pathol* 2000;31:185-92.](#)
44. [Subbiah V, McMahon C, Patel S, Zinner R, Silva EG, Elvin JA, et al. STUMP un"stumped": anti-tumor response to anaplastic lymphoma kinase \(ALK\) inhibitor based targeted therapy in uterine inflammatory myofibroblastic tumor with myxoid features harboring DCTN1-ALK fusion. *Journal Hematol Oncol* 2015;8:66.](#)
45. [Lee BY, Timpson P, Horvath LG, Daly RJ. FAK signaling in human cancer as a target for therapeutics. *Pharmacol Ther* 2015;146:132-49.](#)
46. [Sulzmaier FJ, Jean C, Schlaepfer DD. FAK in cancer: mechanistic findings and clinical applications. *Nat Rev Cancer* 2014;14:598-610.](#)
47. [Ren H, Tan ZP, Zhu X, Crosby K, Haack H, Ren JM, et al. Identification of anaplastic lymphoma kinase as a potential therapeutic target in ovarian cancer. *Cancer Res* 2012;72:3312-3323.](#)
48. [Petricoin EF, Espina V, Araujo RP, Midura B, Yeung C, Wan X, et al. Phosphoprotein pathway mapping: Akt/mammalian target of rapamycin activation is negatively associated with childhood rhabdomyosarcoma survival. *Cancer Res* 2007;67\(7\):3431-40.](#)
49. [Noujaim J, Payne LS, Judson I, Jones RL, Huang PH. Phosphoproteomics in translational research: a sarcoma perspective. *Ann Oncol* 2016;27\(5\):787-94.](#)
50. [Palmer RH, Vernersson E, Grabbe C, Hallberg B. Anaplastic lymphoma kinase: signalling in development and disease. *Biochem J* 2009;420:345-61.](#)

Table 1. Sarcoma cell line characteristics

Age group	Type	Tissue type	Cell line	Translocation	Translocation details	Subtype	Prognosis	Age at diagnosis	Sex	Primary site/specimen	Metastatic site	Ref ^a	
Pediatric / AYA	ES	Bone	ES1	EWS-FLI1	Exon 7/5; Type II			45	F	Left thigh/same	?	*	
			ES2	EWS-FLI1	Exon 10/6; Type III			14	F	Ilium/bone marrow	Bone marrow	*	
			ES4	EWS-FLI1	Exon 7/5; Type II			18	M	Right 8 th rib	Pleural cavity	*	
			ES7	EWS-FLI1	Exon 10/5			15	M	Right fibula lesion	Bone marrow, liver, femur	*	
			ES8	EWS-FLI1	Exon 7/5; Type II			10	M	Left proximal humerus lesion	Femur	*	
			EW8	EWS-FLI1	Exon 7/6; Type I			17	M	Abdominal mass		*	
	RMS	STS	RD				eRMS	Int.	7	F	Pelvic mass		(1 ^a)
							eRMS	Int.	2	F	Perineum		(2 ^a)
				Rh30	PAX3-FKHR		aRMS	Poor	16	M	Soft tissue	Bone marrow	(2 ^a)
				Rh41	PAX3-FKHR		aRMS	Poor	12	F	Soft tissue	Liver	(2 ^a)
				Rh3	PAX3-FKHR		aRMS	Poor	16	M	Bone Marrow	Lung	*
				Rh5	PAX3-FKHR		aRMS	Poor	16	M	Bone Marrow		*
	SS	STS	Aska-SS		SS18-SSX1		Biphasic	DOD	27	M	Groin	Lung	(3 ^a)
					SS18-SSX1		Biphasic	DOD	30	M	Thigh	Lung	(3 ^a)
				SS18-SSX2		Biphasic	?	19	F	Groin		(4 ^a)	
				SS18-SSX2		Monophasic	?	18	F	Thigh		(4 ^a)	
Adult	GIST	STS	GIST882					Meta			Metastatic; site unknown	(5 ^a)	
			AS	STS	ISO-HAS-B		Hemangio-sarcoma		84	M	Primary parietal-scalp tumor	Metastatic arterialauricular lesion	(6 ^a)
	MO-LAS-B				Lymphangio-sarcoma	DOD	77	M	Scalp and face	Lung, liver, spleen, adrenal gland, vertebrae, rib, pleura, diaphragm, lymph node	(6 ^a)		

Table 1. Sarcoma cell line characteristics

AYA = adolescent and young adult; STS = soft-tissue sarcoma; ES = Ewing Sarcoma; RMS = rhabdomyosarcoma (a = alveolar, e = embryonal); SS = synovial sarcoma; GIST = gastrointestinal stromal tumor; AS = angiosarcoma; Int = Intermediate; DOD = Dead of disease; ? = unknown; Meta = metastatic. ^a Provided in supplementary references list. * Personal communication with dr. Peter Houghton / Susan Ragsdale of the Pediatric Preclinical Testing Program (PPTP; Columbus, Ohio); St. Jude Childrens Hospital.

Figure legends

Figure 1. Tyrosine phosphorylation profiling of sarcoma cell lines

A. Unsupervised hierarchical clustering of sarcoma cell lines based on tyrosine phosphorylation patterns. In general, the cells clustered into two major groups: 1. adult sarcomas (GIST and AS; Subgroup A) and 2. pediatric/AYA sarcomas (SS, RMS and ES; further divided into Subgroups B and C). Color bars indicate sarcoma subgroups as described in Table 1; tyrosine phosphorylation data used to create this figure are provided in Supplemental Table 4, tab 2). **B.** Protein-protein network analysis of Subgroup A revealing PTK2 (FAK) as key mediator. Red dots indicate hyperphosphorylated proteins found in Subgroup A only. Direct protein-protein interactions are indicated by blue lines, while kinase-substrate relationships are indicated by magenta lines with arrows. **C.** Unsupervised hierarchical clustering using tyrosine kinase-derived phosphopeptides. Tyrosine kinase phosphorylation data used to create this figure are provided in Supplemental Table 4, tab 3.

Figure 2. Tyrosine phosphorylation of specific tyrosine kinases in sarcoma cell lines

A. Contribution of individual tyrosine kinases to total phosphopeptide abundance. Each sector represents the sum of phosphocounts for each TK across all cell lines as a fraction of the total number of phosphotyrosine counts in the whole panel, and n indicates the number of cell lines in the panel where a given kinase was detected at any level (as detailed in Supplemental Table 4; tab 4). Similar colors indicate members of particular TK families. **B.** Phosphorylation profiles of specific TKs across the sarcoma cell line panel. Detailed data are provided in Supplemental Table 4, tab 4. TKs are divided into receptor TKs and non-receptor TKs and grouped in their respective families (14). **C.** ALK expression and phosphorylation in SS cell lines. Lysates were Western blotted with antibodies specific for total ALK and pALK: pY1096, pY1282/pY1283 (= activation loop) and pY1507. Red arrows highlight the hyperphosphorylated 110 kDa ALK variant in Aska-SS. Normal ALK has a mobility of 220 kDa. The asterisk indicates a cross-reacting band. Actin was used as a loading control.

Figure 3. Characterization of the novel ALK driver in Aska-SS cells

A. FISH analysis demonstrating ALK breakage in the Aska-SS cell line. The arrows highlight single red signals indicating the presence of a breakpoint, whereas the other signals comprise both green and red label indicating full length ALK. Image is at x630 magnification. **B.** Discontinuous expression of ALK coding exons in Aska-SS. RNAseq was undertaken following capture of transcripts corresponding to ALK coding regions. Note low expression of exon 1, absent expression of exons 2-17, and then high expression from exon 18 onwards. The black and blue bars represent the mean expression levels for exons 1-17 and 18-29, respectively. **C.** Confirmation of exon 1-exon 18 splicing in Aska-SS. RT-PCR was undertaken on total RNA from Aska-SS and EW8 (harboring full-length ALK). For Aska-SS, Lanes 1, 2, 3 and 4 contain products generated from primers specific for exons 1 (forward) and 18 (reverse) (predicted size for ALK variant: 317 bp), exons 1 and 21 (predicted size for ALK variant: 784 bp), exon 18 and 21 (predicted size for ALK-variant: 415 bp) and exon 1-C-terminal end of coding region (predicted size for ALK-variant: 2098 bp), respectively. The same reactions were undertaken for EW8, but only the exon 18 and 21 primers generate a detectable product as the other fragment sizes are too large in the context of full-length ALK. **D.** Confirmation of exon 1-exon 18 splicing by DNA sequencing. The 317 bp product generated by RT-PCR was subjected to DNA sequencing. The nature of other products in Panel C were also confirmed by this approach. **E.** Schematic representation of the truncated form of ALK in Aska-SS (ALK Δ 2-17). The extracellular domain of full-length ALK comprises two MAM (meprin, A5 protein and receptor protein tyrosine phosphatase mu) domains (aa 264–427 and 480–626), one low-density lipoprotein class A (LDLa) motif (aa 453–471) and a glycine-rich region (aa 816–940) (50). Because exons 2-17 of ALK encode the aa 223–971 region, the deletion results in a truncated form of ALK (ALK Δ 2-17) lacking these four domains. TM = transmembrane; PTK = protein tyrosine kinase.

Figure 4. Validation of ALK as a potential actionable target in SS

A. Effect of ALK inhibitors on SS cell line proliferation *in vitro*. The graphs indicate dose-response curves of SS cell lines to crizotinib, ceritinib and TAE-684 monotherapies. Error bars represent standard deviations. **B.** Effect of crizotinib on key signaling pathways in the Aska-SS cell line. Cells were treated with the indicated concentrations of crizotinib for 1 h. Cell lysates were prepared and Western blotted with the indicated antibodies. Data are representative of duplicate experiments. **C.** Pathscan signaling pathway analysis for Aska-SS cells treated with ALK inhibitors. Cells were treated with TAE684 (25 nM), ceritinib (100 nM) or crizotinib (750 nM) for 24h. All signals were significantly different from control ($p < 0.05$), apart from the trends observed for ceritinib on pAkt Ser473 ($p = 0.0561$), TAE684 on pAkt Thr308 ($p = 0.0728$), TAE684 on pSTAT3 Tyr705 ($p = 0.0636$), and no significant difference for crizotinib on pSTAT1 Tyr701 ($p = 0.1563$). **D-E.** Effect of ALK inhibitors on Aska-SS xenograft growth. Mice were treated with crizotinib (50 mg/kg) (D) or ceritinib (50 mg/kg) (E). Values are presented as mean relative tumor volume \pm Standard deviation. P-values were assessed by Student's t-test **F.** Expression of ALK in human SS. Examples of patient SS sections with positive (left) and negative (right) ALK expression, as determined by IHC. Images are x200 magnification; insets are x400 magnification. **G.** IHC staining of ALK in Aska-SS (positive control for F). Image is at x200 magnification. **H.** FISH analysis demonstrating ALK breakage in a SS patient. The arrows highlight single colored signals indicating a breakpoint. Image is at x100 magnification.

Figure 5. Targeting of MET and PDGFR α in *in vitro* and *in vivo* SS models

A. Effect of pazopanib on SS cell line proliferation *in vitro*. The graph indicates dose-response curves for the different cell lines. Error bars represent standard deviations. **B.** Expression of total MET and PDGFR α RTKs in the four SS cell lines. For MET, the 145 kDa band represents mature, processed MET, the upper band seen in Yamato-SS is pro-MET. **C.** Synergism between pazopanib and crizotinib treatment in the Yamato-SS cell line *in vitro*. The x-axis and y-axis, respectively, show the relative concentration of pazopanib and crizotinib in synergy compared to the concentrations required in

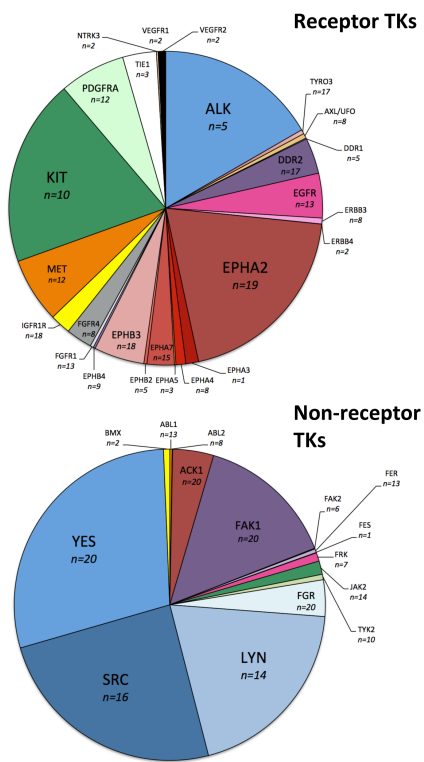
monotherapy to obtain a similar effect on SS cell viability (concentration combination/concentration monotherapy) (details in Methods). The bold line represents a combination index of 1. Dots below, on or above the bold line represent synergy, additivity or antagonism, respectively. Numbers next to the dots indicate the concentrations of pazopanib (nM; left) and crizotinib (nM; right) used in the combinations. **D.** Effect of pazopanib and crizotinib, alone and in combination, on key signaling pathways in Yamato-SS cells. Cells were treated with the indicated concentrations of pazopanib and crizotinib for 1 h. Cell lysates were prepared and Western blotted with the indicated antibodies. Data are representative of duplicate experiments. **E.** Pathscan signaling pathway analysis for Yamato-SS cells treated with pazopanib and/or crizotinib. Cells were treated with crizotinib (250nM) and/or pazopanib (10 μ M) for 24h. All signals were significantly different ($p < 0.05$) versus control, apart from combination treatment on pAkt Thr308 ($p = 0.102$) and pazopanib pStat3 Tyr705 ($p = 0.0825$). With combined treatment, the reduction in pAkt Ser473 and STAT1 Tyr701 was significant compared to both monotherapies and control (all $p < 0.01$; Student's t-test). **F.** Effect of pazopanib and crizotinib, alone and in combination, on anchorage-independent growth of Yamato-SS cells. Error bars represent standard deviation, p-values were obtained with Student's t-test. **G.** Effect of crizotinib on Yamato-SS xenograft growth. Mice were treated with the indicated concentrations of crizotinib. Values are presented as mean relative tumor volume \pm SEM. *: $p < 0.05$; **: $p < 0.01$; ***: $P < 0.001$ as assessed by Student's t-test. **H.** Effect of pazopanib on Yamato-SS xenograft growth. Values are presented as in G. *: $p < 0.05$; **: $p < 0.01$ as assessed by Student's t-test. **I.** Effect of pazopanib on angiogenesis. CD34 expression in Yamato-SS tumors from the pazopanib treatment group (100mg/kg) (top) and control group (bottom). Images are x100 magnification.

Figure 6. MET and PDGFR α expression in SS patient tumors

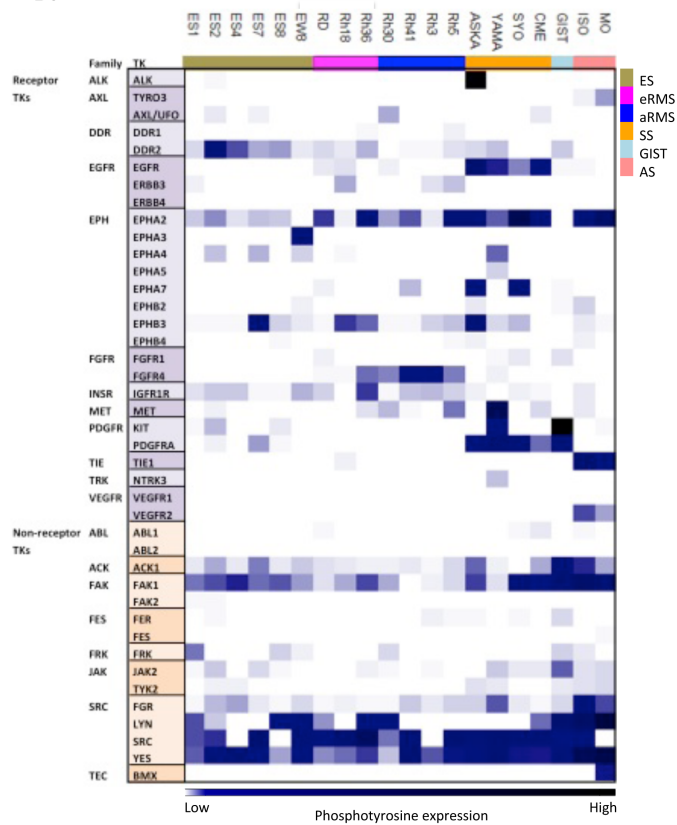
A and B: Examples of patient SS sections with positive (left) and negative (right) MET and PDGFR α expression, respectively. **C.** Example of a patient with a biphasic, primary SS. Expression of MET in the epithelial cells (left) and PDGFR α in the mesenchymal cells (middle) is evident. General morphology is demonstrated by H&E staining (right). Images are x200 magnification; insets are x400 magnification.

Fig. 2

A.



B.



C.

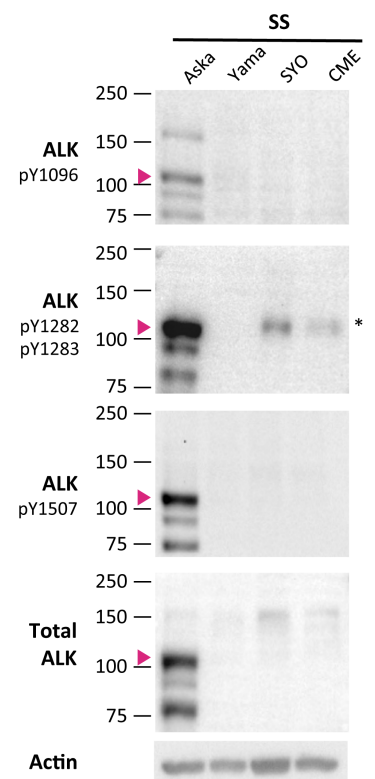


Fig. 3

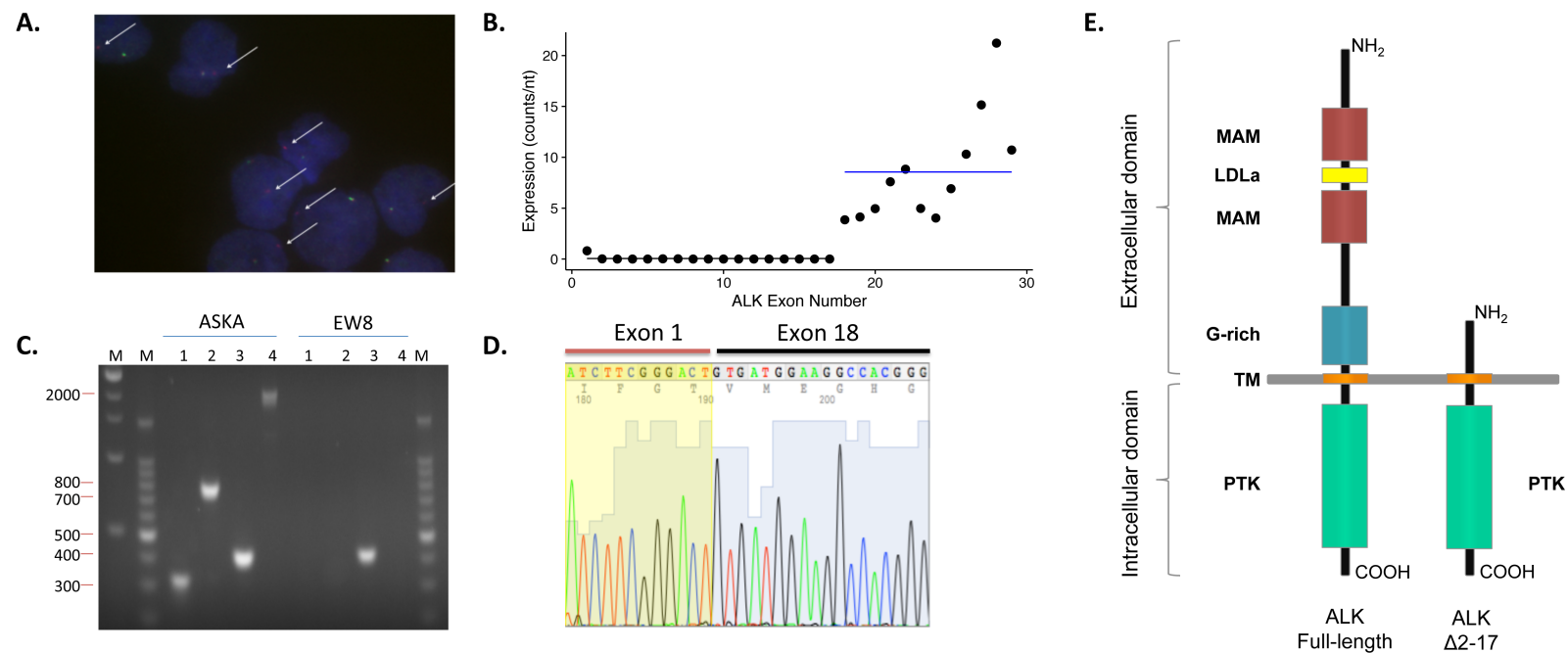


Fig. 4

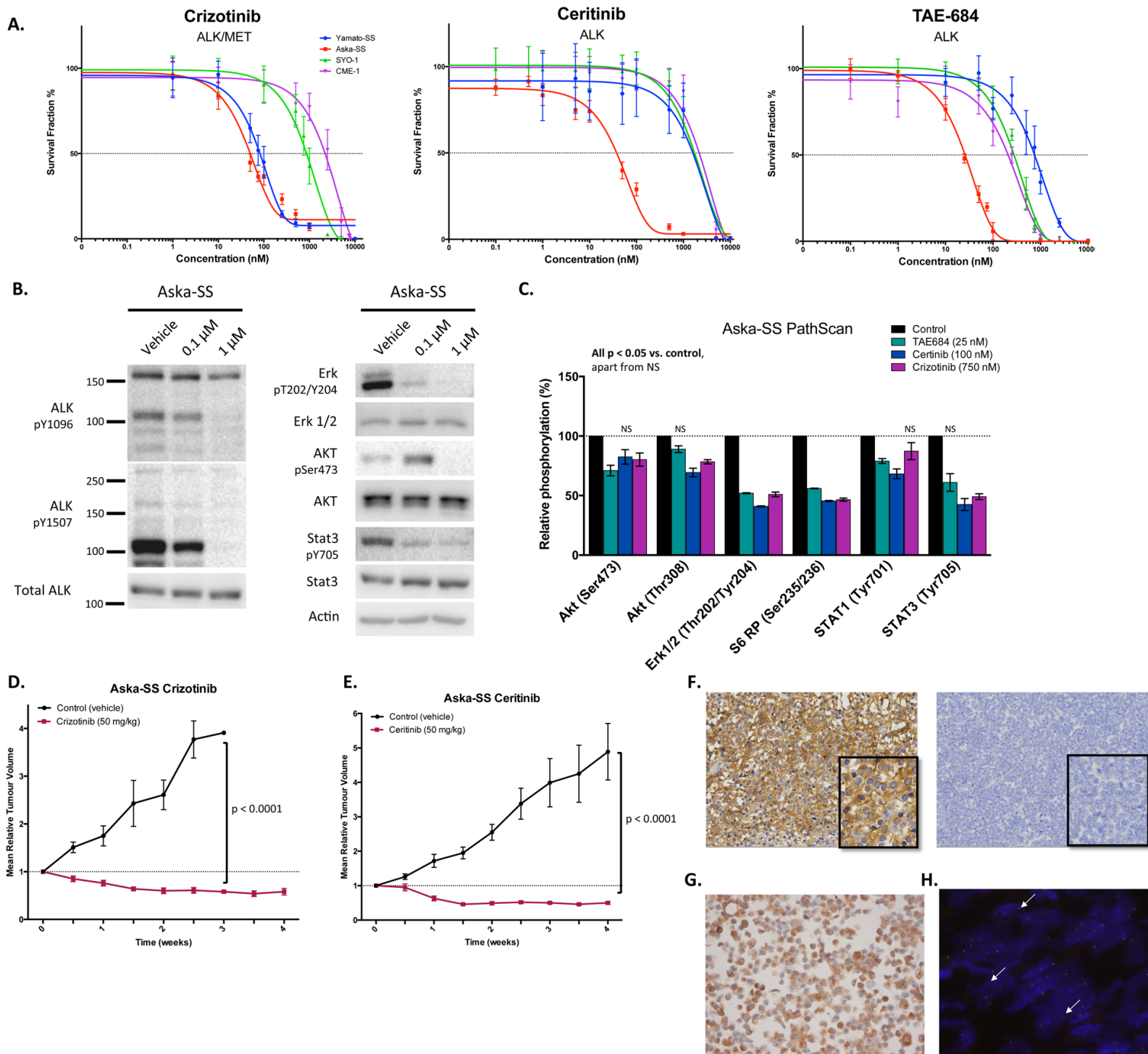


Fig. 5

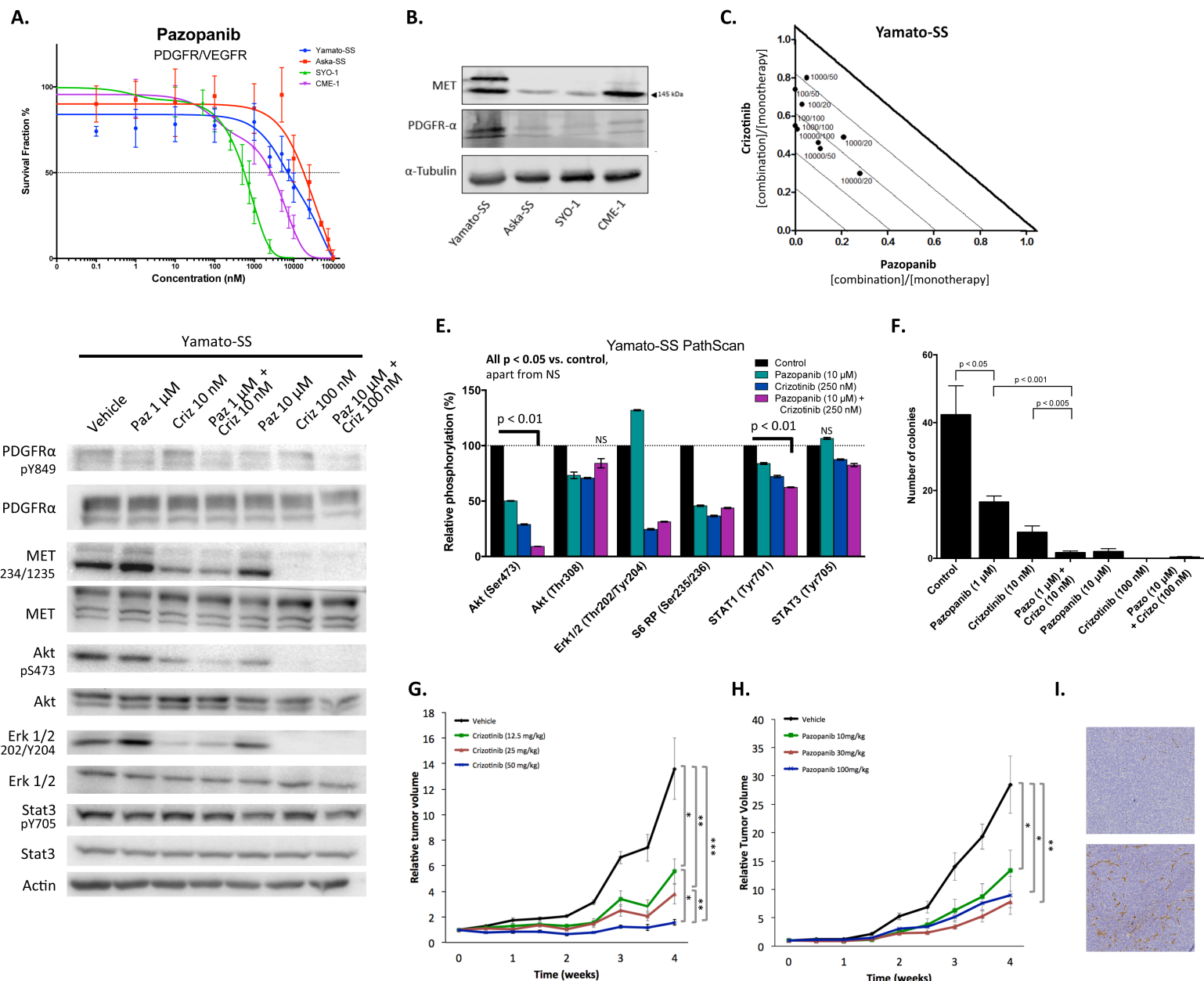
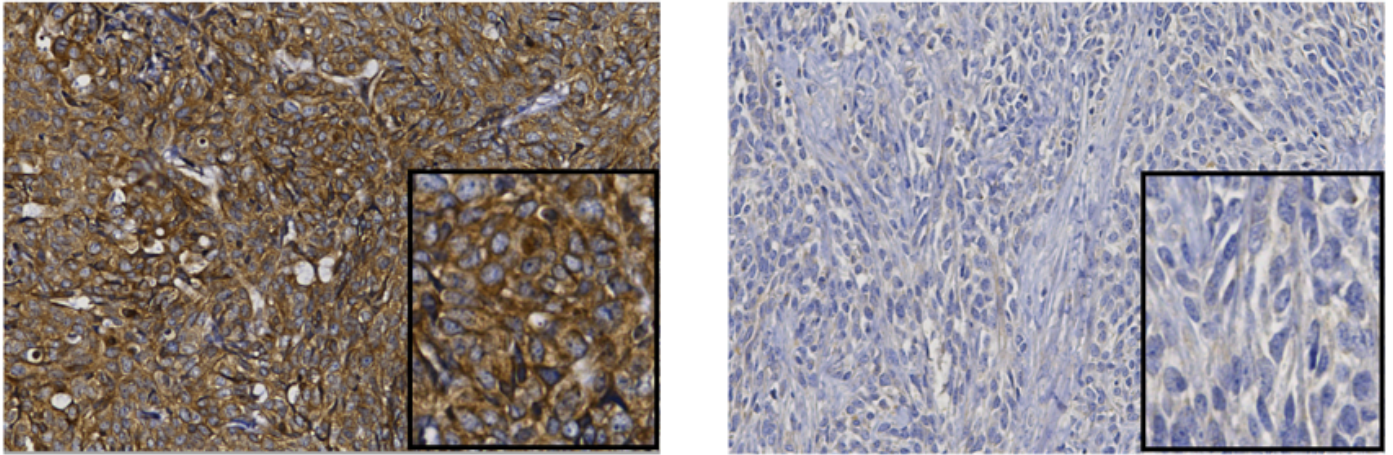
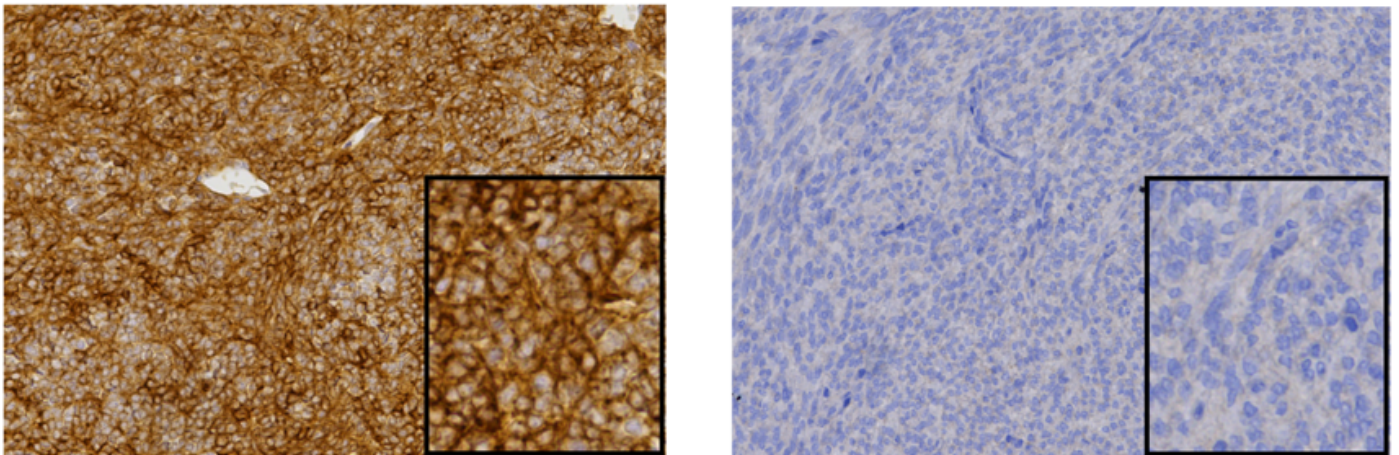


Fig.6

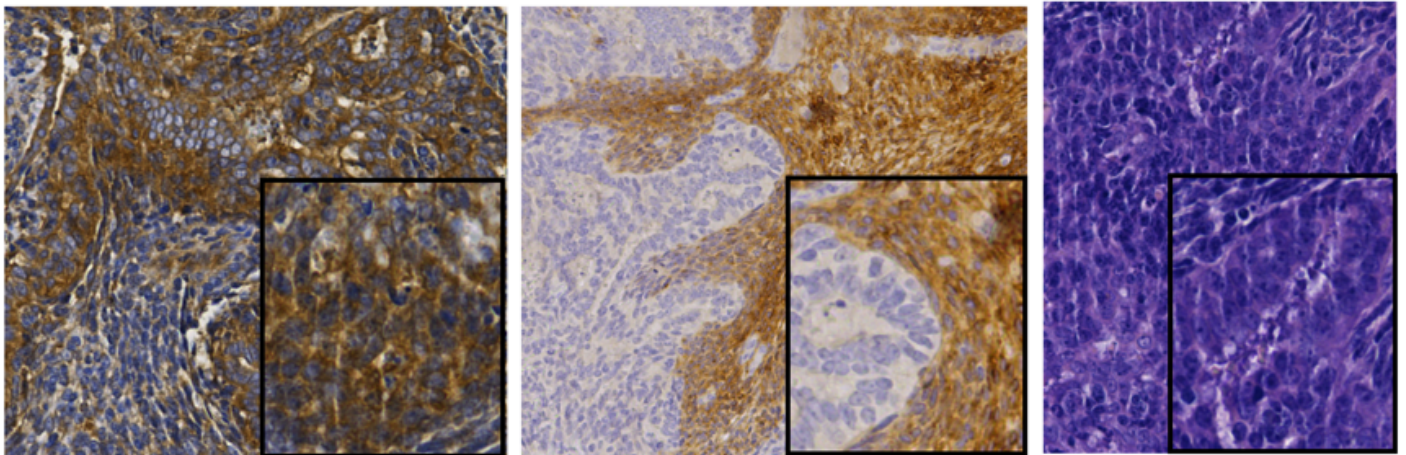
A.



B.



C.



Cancer Research

The Journal of Cancer Research (1916–1930) | The American Journal of Cancer (1931–1940)

Phosphoproteomic profiling reveals ALK and MET as novel actionable targets across synovial sarcoma subtypes

Emmy D.G. Fleuren, Myrella Vlenterie, Winette van der Graaf, et al.

Cancer Res Published OnlineFirst June 20, 2017.

Updated version	Access the most recent version of this article at: doi: 10.1158/0008-5472.CAN-16-2550
Supplementary Material	Access the most recent supplemental material at: http://cancerres.aacrjournals.org/content/suppl/2017/06/17/0008-5472.CAN-16-2550.DC1

E-mail alerts [Sign up to receive free email-alerts](#) related to this article or journal.

Reprints and Subscriptions To order reprints of this article or to subscribe to the journal, contact the AACR Publications Department at pubs@aacr.org.

Permissions To request permission to re-use all or part of this article, contact the AACR Publications Department at permissions@aacr.org.